Genetic landscape and autoimmunity of monocytes in developing Vogt–Koyanagi–Harada disease

Youjin Hu[a,1], Yixin Hu[a,1], Yuhua Xiao[a,1], Feng Wen[a], Shaochong Zhang[a], Dan Liang[a], Lishi Su[a], Yang Deng[a], Jiawen Luo[a], Jingsong Ou[b], Mingzhi Lu[a], Yanhua Hong[a], and Wei Chi[a,2]

[a]State Key Laboratory of Ophthalmology, Zhongshan Ophthalmic Centre, Sun Yat-sen University, 510060 Guangzhou, China; and [b]Division of Cardiac Surgery, Heart Center, The First Affiliated Hospital, Sun Yat-sen University, 510080 Guanzhou, China

Edited by Lawrence Steinman, Stanford University School of Medicine, Stanford, CA, and approved August 31, 2020 (received for review February 9, 2020)

Vogt–Koyanagi–Harada (VKH) disease is a systemic autoimmune disorder affecting multiple organs, including eyes, skin, and central nervous system. It is known that monocytes significantly contribute to the development of autoimmune disease. However, the subset heterogeneity with unique functions and signatures in human circulating monocytes and the identity of disease-specific monocytic populations remain largely unknown. Here, we employed an advanced single-cell RNA sequencing technology to systematically analyze 11,259 human circulating monocytes and genetically defined their subpopulations. We constructed a precise atlas of human blood monocytes, identified six subpopulations—including S100A12, HLA, CD16, proinflammatory, megakaryocyte-like, and NK-like monocyte subsets—and uncovered two previously unidentified subsets: HLA and megakaryocyte-like monocyte subsets. Relative to healthy individuals, cellular composition, gene expression signatures, and activation states were markedly alternated in VKH patients utilizing cell type-specific programs, especially the CD16 and proinflammatory monocyte subpopulations. Notably, we discovered a disease-relevant subgroup, proinflammatory monocytes, which showed a discriminative gene expression signature indicative of inflammation, antiviral activity, and pathologic activation, and converted into a pathologic activation state implicating the active inflammation during VKH disease. Additionally, we found the cell type-specific transcriptional signature of proinflammatory monocytes, ISG15, whose production might reflect the treatment response. Taken together, in this study, we present discoveries on accurate classification, molecular markers, and signaling pathways for VKH disease-associated monocytes. Therapeutically targeting this proinflammatory monocyte subpopulation would provide an attractive approach for treating VKH, as well as other autoimmune diseases.

Vogt–Koyanagi–Harada disease | single-cell RNA sequencing | monocyte subsets | ISG15

Vogt–Koyanagi–Harada (VKH) disease is one of the common sight-threatening uveitis entities in the Asian population and carries a high risk of blindness (1). It is a systemic refractory autoimmune disease, affecting multiple organs and characterized by bilateral granulomatous panuveitis and systemic disorders, including leukoderma, paratrichosis, and various central nervous system and auditory signs (2). While the clinical features and diagnostic criteria are well described, the pathogenesis of VKH disease remains unclear. Moreover, there are currently no reliable disease-specific biomarkers to objectively and accurately evaluate the in vivo immune status at different disease stages and predict the response to treatment. Evidence accumulated over the past few decades suggests that VKH disease occurs in individuals with a predisposing genetic background. Indeed, several susceptibility genes have been identified, such as HLA-DR4 and HLA-DRw53 (3). It is speculated that activation of antigen-specific T cells contributes to the adaptive immune responses driving VKH disease pathogenesis (4). However, it is unclear how triggering factors initiate the innate immune responses and ensuing chronic adaptive immune melanocyte attack in multiple organs characteristic of VKH disease. Circulating monocytes and tissue-resident macrophages, as well as dendritic cells (DCs) and B cells, are the predominant antigen-presenting cells and are intimately involved in various inflammatory diseases, as well as in tumor development and angiogenesis (5–8). Due to the difficulty in collecting eye tissue samples from uveitis patients (such as inflamed uveal tract or retina), our understanding of immune pathogenesis comes mainly from analysis of peripheral blood leukocytes. In human autoimmune diseases, such as multiple sclerosis and rheumatoid arthritis, monocytes sense inflammatory environmental changes, spread inflammation at a systemic level, and promote the abnormal production of immune factors (8, 9). Furthermore, the interactions among monocytes of the innate immune system and antigen-specific cells of the adaptive immune system are seminal to the inflammatory processes underlying experimental autoimmune uveitis (EAU), a well-characterized model for autoimmune uveitis (10). However, little is known about the contributions of specific monocyte populations to human uveitis. We therefore sought to describe the landscape of monocyte subsets and specific gene expression signatures in greater detail to identify pathogenic contributions and biomarkers for VKH disease activity and treatment response.

Monocyte subsets are defined principally by surface expression patterns using flow cytometry and by functional profiling according to cytokine induction (11, 12). However, these analytic approaches are biased by the limitations of limited markers available to identify, isolate, and manipulate the cells, strongly relying on

Significance

Vogt–Koyanagi–Harada (VKH) disease is one of the most common and severe vision-threatening autoimmune uveitis in Asians. However, the functional heterogeneity among subsets in human blood monocytes and the VKH disease-relevant populations remains elusive. This study encoded the landscape of human monocytes, clustered six subsets with distinct functions, and revealed two populations, using single-cell RNA sequencing. Surprisingly, we discovered a disease-specific subset, proinflammatory monocytes, implicating immune activation in VKH disease. We also identified a cell type-specific transcriptional signature in subset ISG15, which might be corresponded with treatment response. These data highlight advanced understanding of pathogenesis, mapping an atlas of autoimmune monocytes and potential therapeutic targets in autoimmune uveitis.

Author contributions: Youjin Hu and W.C. designed research; Youjin Hu, Yixin Hu, Y.X., and W.C. performed research; Youjin Hu and W.C. contributed new reagents/analytic tools; Youjin Hu, Yixin Hu, Y.X., F.W., S.Z., D.L., L.S., Y.D., J.L., J.O., M.L., Y.H., and W.C. analyzed data; and Youjin Hu, Yixin Hu, Y.X., and W.C. wrote the paper.

The authors declare no competing interest.

This article is a PNAS Direct Submission.

[1]Youjin Hu, Yixin Hu, and Y.X. contributed equally to this work.

[2]To whom correspondence may be addressed. Email: chiwei@mail.sysu.edu.cn.

This article contains supporting information online at https://www.pnas.org/lookup/suppl/doi:10.1073/pnas.2002476117/-/DCSupplemental.

First published September 28, 2020.

high-quality antibodies to merely reveal the information of pooled cell populations. In the present study, we used the latest advanced technology, single-cell RNA sequencing (scRNA-seq), termed as an ongoing technological revolution, to break the border limitations of traditional analysis manners and enable the rapid determination of precise gene expression patterns of several thousands of individual cells in an unbiased fashion, leading to define accurate classification, identify subsets, and uncover the cellular composition and signatures of human blood monocytes. Moreover, we reveal the contributions of the monocyte subtypes with unique inflammatory functions determining immune responses, provide evidence for the hypotheses of VKH disease pathogenesis, and have discovered a molecule to monitor the therapeutic efficacy.

Results

Clustering Analysis of Blood Monocytes and Cell Population Identification. To generate a more detailed molecular atlas of human monocytes, we isolated monocytes from peripheral blood mononuclear cells (PBMCs) by negative magnetic beads to sort unlabeled cells of monocytes and conducted droplet-based scRNA-seq (Fig. 1*A*). We first sequenced 15,606 high-quality sorted cells from three healthy donors, identified the 2,000 genes with the highest expression variability among these cells (*SI Appendix*), and performed principal component analysis (PCA). The 46 significant PCs were reduced to two dimensions using t-distributed stochastic neighbor embedding (t-SNE) methods for visualization. Eleven cell clusters were identified by unsupervised analysis using a graph-based approach (Fig. 1*B*). Differential expression analysis was performed among each cluster, and subpopulations were defined by comparing unique gene expression patterns with those of published reference cell clusters in blood samples from healthy individuals (Table 1 and Fig. 1 *C* and *D*). Two clusters mapped closely to monocytes, one to $CD14^{high}$ monocytes and the other to $CD16^{high}$ monocytes. In addition, two clusters exhibited the gene expression characteristics of $CD1c^{+}$ DC and plasmacytoid (p) DC populations, respectively, while one cluster corresponded to megakaryocyte progenitor cells. One population also corresponded to nonspecific immunity natural killer (NK) cells, and four corresponded to specific immunity B lymphocytes, T lymphocytes, NKT lymphocytes, and plasma cells.

A previous study by Villani et al. profiled 372 single blood monocytes from one donor via scRNA-seq (22). In this study, the number of monocytes is 11,259, providing an unprecedented opportunity to yield numerous discriminative genes to characterize the functions and activation states of each subset. Analysis of $CD14^{high}$ monocytes, which included classical and intermediate monocytes, not only validated markers reported in previous studies (*S100A12, S100A8, S100A9, VCAN, LYZ, CD14, FCB1,* and *MNDA*) (23–26) but also identified a number of markers such as *CSTA, MS4A6A, CXCL8, CTSS, LGALS1, LGALS2,* and *CST3*. For $CD16^{high}$ monocytes, known as nonclassical monocytes, this high-throughput analysis also confirmed previously recognized genes (*FCGR3A, TCF7L2, MS4A7, RHOC, IFITM3,* and *CSF1R*) (22) and identified the distinguishing biomarkers *CDKN1C, HES4, SMIM25, MTSS1, BCL2A1,* and *RRAS*. To examine the relationships between other clusters and monocytes, we profiled DCs (including 736 $CD1c^{+}$ DCs and 126 pDCs), lymphocytes (including 549 T cells, 723 NKT cells, 724 NK cells, 190 B cells, and 393 plasma cells), and 628 megakaryocyte progenitors. Like monocytes, DCs, B lymphocytes, and plasma cells present antigens to downstream cells, and, consistent with this function, all expressed various HLA-associated genes, such as *HLA-DPA1, HLA-DPB1, HLA-DQA1,* and *HLA-DQB1*. In addition, $CD1c^{+}$ DCs, $CD16^{high}$ monocytes, NK cells, and NKT cells coexpressed *RHOC*, a member of the Rho subfamily GTPases involved in actin dynamics, vesicular trafficking, gene transcription, cell cycle progression, and cell adhesion. Both B cells and $CD16^{high}$ monocytes also coexpressed *CD79B*, which was previously thought to be expressed only by B lymphocytes and effector B cells (plasma cells). In addition, *FCGR3A*/CD16 was highly expressed in NK and NKT cells; thus, the combination of these marker genes can be used to identify $CD16^{high}$ monocytes with greater precision than *FCGR3A*/CD16 alone. In contrast, megakaryocyte progenitors and T cells expressed few genes in common with monocytes.

In summary, by measuring the gene expression profile in a large number of individual sorted PBMCs, we identified numerous discriminative genes for two conventional monocyte populations. In addition, we identified multiple genes coexpressed in monocytes and other components of PBMCs, suggesting overlapping functions.

Single-Cell Profiling of Human Circulating Monocytes. Monocytes were initially divided into two categories, CD16-expressing and non–CD16-expressing, and CD16-expressing monocytes were subsequently subdivided into two groups by CD14 expression, forming the current taxonomy consisting of classical monocytes ($CD14^{++}$ $CD16^{-}$), intermediate monocytes ($CD14^{++}$ $CD16^{+}$), and nonclassical monocytes ($CD14^{dim}$ $CD16^{++}$) (27). To further describe the heterogeneity of human blood monocytes at the single-cell level and provide additional markers for more precise subset classification, we profiled 11,259 circulating monocytes. We identified six populations (Fig. 2*A*) with two previously unreported subsets according to similarities and differences in transcriptome profiles (*SI Appendix*). Based on the expression pattern of CD14 and *FCGR3A*/CD16 (Fig. 2*B*), we classified five subpopulations as $CD14^{high}$ and one as $CD16^{high}$ monocytes. We also noticed a group of cells located at the junction of $CD14^{high}$ monocytes and $CD16^{high}$ monocytes on the Uniform Manifold Approximation and Projection (UMAP) belonging to a small part of a subpopulation of $CD14^{high}$ monocytes. Based on high CD14 and moderate *FCGR3A*/CD16 expression, these cells mapped closely to intermediate monocytes. Although they could not be clustered unbiasedly into a single subgroup, their location on the UMAP supported the view that they were likely in the transition state from classical to nonclassical. We further characterized each cluster by the top 10 marker genes (Fig. 2 *C* and *D*). The S100A12 monocytes represented the commonalities among $CD14^{high}$ monocytes and expressed hallmark proinflammatory mediators, including *S100A8* and *S100A9*, in addition to *S100A12*. Another subset, HLA monocytes, expressed the MHC Class II molecules *LGALS2* and *CPVL*. Although HLA-associated genes were also expressed by other subsets, this HLA subset possessed the most diverse and highest levels of HLA-related gene expression, including unique expression of *HLA-DMA* and *HLA-DMB*, indicating the strongest antigen processing and presentation capacities among $CD14^{high}$ monocytes. In contrast to $CD14^{high}$ monocytes, CD16 monocytes were a nonclassical population. In addition to confirming expression of FCGR3A, we also identified *CDKN1C, TCF7L2, RHOC, HES4, IFITM2, IFITM3, MS4A7, MTSS1, SMIM25, HLA-DPA1/B1*, and *HLA-DRB1* as selective molecular markers, suggesting that this population was enriched in negative regulators of cell proliferation, as well as genes related to the Wnt signaling pathway, actin organization, Notch signaling pathway, type I interferon (IFN) antiviral response, and homeostasis of the nervous system (28–33). Proinflammatory monocytes presented a unique combination of genes, including chemokine ligands, interleukins, and nod-like receptors (e.g., *CCL3, CCL4, IL1B,* and *NLRP3*) associated with virus infection, the inflammatory process, and pyroptotic cell death (34–36). Megakaryocyte-like monocytes expressed genes similar to megakaryocyte progenitors (including *PPBP* and *PF4*), indicating functions in the activation of platelets and inflammation, as well as megakaryocytes (37, 38). NK cell-like monocytes expressed a cytotoxic gene signature (e.g., *GZMA* and *GNLY*) (39) and shared

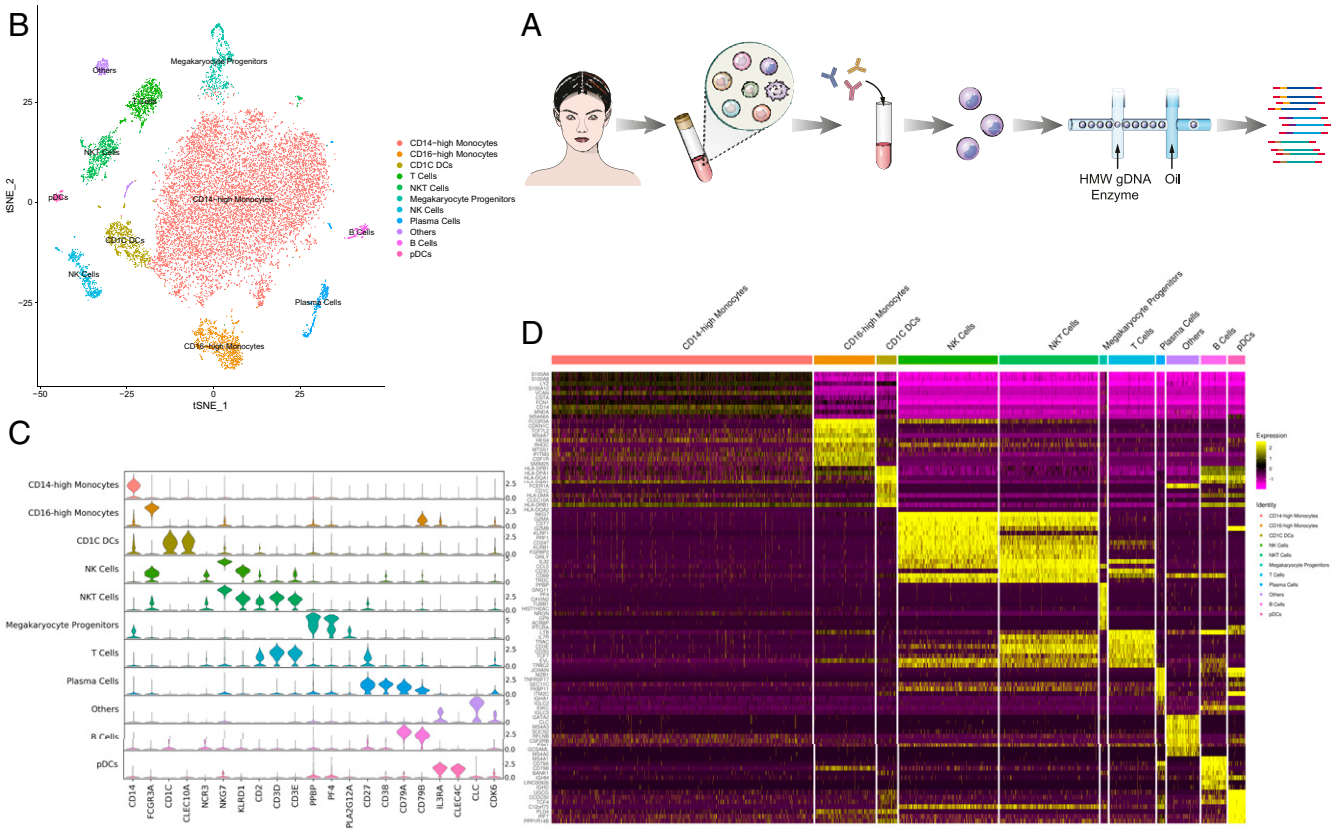

Fig. 1. Clustering analysis of blood monocytes and cell population identification. (*A*) The procedure of scRNA-seq. (*B*) The 15,606 cells are clustered into 11 clusters based on their expression pattern. Their putative identities are annotated on the right. Colors indicate unbiased classification via graph-based clustering. Each dot represents an individual cell. Numbers of successfully profiled single cells per cluster are as follows: monocytes (n = 11,259), CD1c$^+$ DCs (n = 736), pDCs (n = 126), T cells (n = 549), NKT cells (n = 723), NK cells (n = 724), B cells (n = 190), plasma cells (n = 393), and megakaryocyte progenitors (n = 628). (*C*) Violin plots illustrate expression levels of marker genes. The distribution of the cell type-specific marker genes in all clusters of their healthy donors reflects their cell identities. (*D*) The heat map reports scaled expression of discriminative gene sets for each cluster defined in *A*. Up to 10 discriminators of each cluster are listed next to each cluster. The color scheme is based on z-score distribution from −2.5 (purple) to 2.5 (yellow). HMW gDNA, high-molecular-weight genomic DNA.

other differentially expressed genes with NK cells (e.g., *KLRB1* and *NKG7*), indicating the overlapping functions between these population and NK cells. In summary, we demonstrated that human blood monocytes can be reclassified into six subsets instead of the conventional three. Among these subsets, we first identified two subsets (namely, HLA monocyte subsets and megakaryocyte-like monocyte subsets), which was attributed to our analysis of large quantities of human circulating monocytes. Moreover, each subset possessed unique gene expression signatures, indicating specific functions. In addition, intermediate monocytes constituted a small subset within the HLA monocyte group and thus appeared to represent the conversion from classical to nonclassical monocytes.

Mapping Monocyte Atlas of VKH Patients Compared with the Healthy Controls. Monocytes are strongly implicated in the development of autoimmune diseases, but their precise functions, subset classifications, cellular and molecular signatures, and activation states in VKH disease are still obscure. To identify the heterogeneity and alternations of cell composition, we performed droplet-based scRNA-seq and sequenced 23,937 high-quality monocytes from three initial VKH patients with acute uveitis without supervision and compared expression patterns to healthy control monocytes (*SI Appendix*). In accord with findings in the healthy population, patient monocytes were still clustered into six populations (Fig. 3*A*) based on differential gene expression.

The most distinguishing expression changes among all monocyte subsets in VKH disease patients compared to healthy donors was the emergence of transcriptional programs associated with a proinflammatory state (Fig. 3*B* and *SI Appendix*). Proinflammatory monocytes exhibited the largest number of gene expression changes among subtypes, including both up-regulated and down-regulated genes. These results suggested that proinflammatory monocytes may actively participate in the development of VKH disease. Genes with greater than twofold higher expression in VKH patients compared to healthy individuals included *RPS4Y1*, a member of the S4E family of ribosomal

Table 1. Markers of each cell type

Potential cell type	Markers
CD14^{high} monocytes	CD14
CD16^{high} monocytes	FCGR3A
CD1c DCs	CD1C, CLEC10A (13)
NK cells	NCR3, NKG7, KLRD1 (14–16)
T cells	CD2, CD3D, CD3E (17)
NKT cells	CD2, CD3D, CD3E, NCR3, NKG7, KLRD1
Megakaryocyte progenitors	PPBP, PF4, PLA2G12A (18)
Plasma cells	CD27, CD38 (19)
B cells	CD79A, CD79B (20)
pDCs	IL3RA, CLEC4C (21)

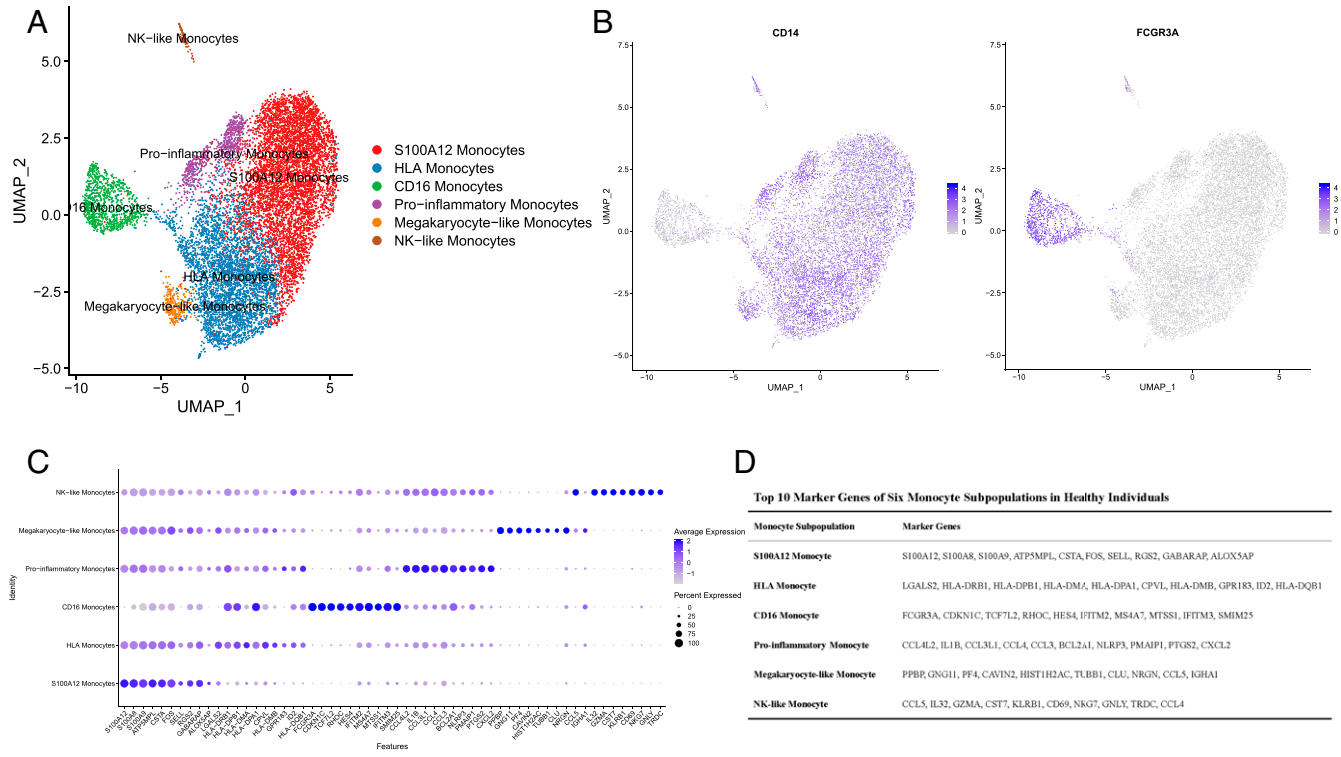

Fig. 2. Single-cell profiling of human circulating monocytes. (*A*) UMAP visualization of the transcriptional heterogeneity of human circulating monocytes. The 11,259 monocytes are further divided into six subsets, and their names are annotated on the right. Different colors are used to distinguish each cluster. Numbers of successfully profiled single cells per subset are as follows: S100A12 monocytes (mono) (n = 5,499), HLA mono (n = 3,799), CD16 mono (n = 901), proinflammatory mono (n = 680), megakaryocyte-like mono (n = 299), and NK-like mono (n = 80). (*B*) Expression pattern of two marker genes (CD14 and CD16/FCGR3A) of human monocytes. Purple is used to represent the expression of these two marker genes, and each dot represents an individual cell. (*C*) Dot plot shows the top 10 marker genes revealed by scRNA-seq of monocyte subsets defined in *A*. (*D*) Top 10 marker genes of six monocyte subpopulations in healthy individuals are listed in the table.

proteins (40), and *TXNIP*, an endogenous inhibitor of the thioredoxin (TRX) system up-regulated in ischemic stroke and other brain diseases (e.g., Alzheimer's disease) and mediating redox/glucose-induced stress and inflammation (41, 42). The significant up-regulation of TXNIP in VKH patients may be related with this disease. Other up-regulated genes included *FOS, ISG15, LY6E,* and *MX1*. These genes were associated with multiple biological processes, such as virus infection, type-I IFN signaling, and responses to IFN-gamma (Fig. 3*D*). According to the Kyoto Encyclopedia of Genes and Genomes (KEGG) database, these up-regulated genes were mainly associated with T-helper cell differentiation, infectious diseases caused by viruses and bacteria (e.g., influenza A, viral myocarditis, Leishmaniasis, *Salmonella* infection), autoimmune diseases (e.g., graft-versus-host disease, autoimmune thyroid disease, allograft rejection), and inflammatory diseases (e.g., rheumatoid arthritis and inflammatory bowel disease) (Fig. 3*E*). Alternatively, down-regulated genes in VKH patient monocytes mainly included *CCL3, CCL4, CXCL2, CXCL8, TNF, IL1B*, and *NLRP3*. All these changes were consistent with two of the mainstream hypotheses that viral infection (43) may be an inducer to initiate VKH disease and emphasize the critical role of immune response in the pathogenesis of disease. The population with the next greatest number of altered genes was CD16 monocytes (nonclassical monocytes). Previous studies reported that nonclassical monocytes ($CD14^{dim}$ $CD16^{++}$, CD16 monocytes) had controversy toward the functions in different autoimmune diseases. Wong et al. reported that nonclassical monocytes produced high levels of TNF-α and IL-1β, indicating their inflammatory potentials (44). However, Cros et al. reported that CD16 monocytes did not produce reactive oxygen species (ROS), did not express inflammatory chemokine receptors such as CCR2, expressed lower levels of CCR1, CCR5, and IL-17RA, gave little response to lipopolysaccharide (LPS), and, in contrast, expressed higher amounts of IL-1 receptor antagonist, IL-10 receptor, and CXCL16 scavenger receptor, indicating that they were antiinflammatory (45). In our present study, up-regulated genes included *RPS4Y1, S100A8*, and *S100A9*, involved in protein synthesis and modulation of inflammatory responses through migration and chemotaxis of granulocytes and neutrophils (Fig. 3*F*). The down-regulated gene set was similar to that in proinflammatory monocytes (e.g., including *CCL3, CCL4, IL1B,* and *TNF*). Functional annotation analysis indicated that these CD16 monocytes might play dual roles in the regulation of the inflammatory response, the intrinsic apoptotic signaling pathway, the response to external stimulus, and cell chemotaxis and migration. Notably, CD16 monocytes from patients highly expressed NF-κB transcription factors and chemokine production (Fig. 3 *F* and *G*). Hence, $CD14^{high}$ monocytes, especially proinflammatory monocytes, promoted inflammation and the immune response, and CD16 monocytes may have dual effects in the development of VKH disease.

The Production of ISG15 in VKH Patients Was Reduced after Immunosuppressive Therapy. In the above analysis, proinflammatory monocytes demonstrated the greatest gene expression changes in the acute stage of VKH disease, suggesting that phenotypic alterations of this subpopulation may be related to VKH disease development. We therefore focused further analyses on this defined proinflammatory subset, inflammatory monocytes. Although clinical measures can monitor disease activity and treatment response, such as fluorescein fundus angiography (FFA) and optical coherence

tomography (OCT), these assessments yield little information on pathogenic processes, immune status, or the mechanisms underlying treatment responses. To identify a blood-based index of VKH disease, we examined IFN-stimulated gene 15 (ISG15), which specifically highly expressed in the proinflammatory monocytes. Previous studies have shown that ISG15, a member of the ubiquitin family, inhibits the

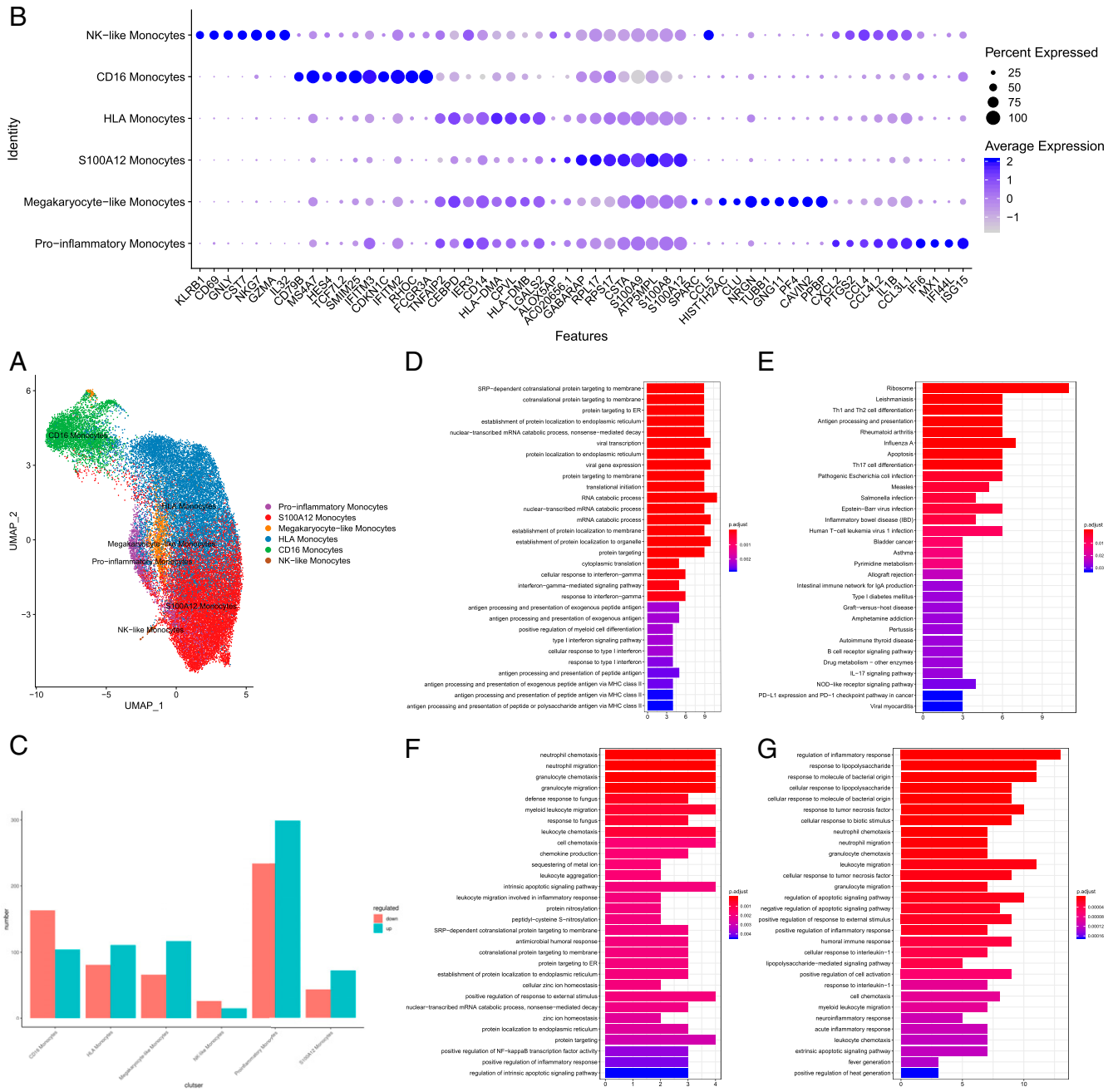

Fig. 3. Mapping monocyte atlas of VKH patients compared with the healthy controls. (*A*) UMAP visualization of the transcriptional heterogeneity of comparing circulating monocytes from three acute VKH patients and healthy donors. A total of 35,483 monocytes are divided into six subpopulations according to the subsets defined in Fig. 2*A*. Different colors are used to distinguish each cluster. Numbers of successfully profiled single cells per subpopulation are as follows: S100A12 mono (n = 13,534), HLA mono (n = 14,537), CD16 mono (n = 4,309), proinflammatory mono (n = 1,435), megakaryocyte-like mono (n = 1,565), and NK-like mono (n = 103). (*B*) Dot plot shows the top 10 marker genes revealed by scRNA-seq of monocyte subpopulations. (*C*) Numbers of up- and down-regulated genes of each monocyte subpopulation when comparing the gene expression changes between acute VKH patients and healthy individuals. Numbers of altered genes with log fold-change (FC) >0.5 and adjusted P value <0.05 per subpopulation are as follows: CD16 mono up-regulated genes (n = 104), CD16 down-regulated genes (n = 163), HLA mono up-regulated genes (n = 111), HLA mono down-regulated genes (n = 81), megakaryocyte-like mono up-regulated genes (n = 117), megakaryocyte-like mono down-regulated genes (n = 66), NK-like mono up-regulated genes (n = 15), NK-like mono down-regulated genes (n = 26), proinflammatory mono up-regulated genes (n = 299), proinflammatory mono down-regulated genes (n = 234), S100A12 mono up-regulated genes (n = 72), and S100A12 mono down-regulated genes (n = 43). (*D*) The up-regulated Gene Ontology (GO) term of biological processes in proinflammatory monocytes. The color scheme is based on P value from 0.001 (red) to 0.002 (purple). (*E*) The up-regulated genes of the KEGG database in proinflammatory monocytes. The color scheme is based on P value from 0.01 (red) to 0.03 (purple). (*F*) The up-regulated GO term of biological processes in CD16 monocytes. The color scheme is based on P value from 0.001 (red) to 0.004 (purple). (*G*) The down-regulated GO term of biological processes in CD16 monocytes.

replication of viruses and regulates host immunity (46). Moreover, ISG15 was identified as a marker of synovial fibroblasts associated with immune responses in rheumatoid arthritis via gene screening (47). However, there is no report on the role of ISG15 in VKH disease. In the present study, we explored the production of ISG15 in monocytes from VKH patients (*SI Appendix*) compared to normal healthy monocytes at the single-cell transcriptomic level and found that ISG15 expression was up-regulated predominantly in the proinflammatory monocyte subset from VKH patients (Fig. 4*A*). Hence, we further explored the expression of ISG15 at the protein level in monocytes using an immunocytochemical assay. Our findings showed that ISG15 was located in both the cytoplasm and nucleus of monocytes. Moreover, ISG15 was significantly higher in acute VKH patients with active uveitis than healthy controls. In addition to ISG15, TXNIP, another important up-regulated gene in the proinflammatory monocyte subset from active VKH patients revealed by single-cell sequencing, was also obviously elevated at the protein level. (Fig. 4 *B* and *C*).

Flow cytometry (Fig. 4*D*) also revealed that the expression level of ISG15 in $CD14^{high}$ monocytes (as indicated by mean fluorescence intensity [MFI]) was significantly higher in active VKH patients (295.13 ± 68.22) than healthy individuals (194.17 ± 43.90) and remained elevated in convalescent patients after 1 mo of treatment (348.13 ± 74.69) although the intraocular inflammation appeared reduced according to clinical examination (Fig. 4*F*). However, ISG15 expression markedly decreased after 3 mo of treatment (174.13 ± 64.48) (Fig. 4 *E* and *G*). These results suggested that ISG15 production in circulating monocytes might reflect the treatment response in VKH disease.

ISG15 is one of the most important regulators of host response to viral infection. It has been reported that ISG15 is mainly stimulated by type-I and type-III IFNs via the activation of IFN regulatory factor 9 (IRF9) and phosphorylated signal transducer and activator of transcription (STAT) 1 and STAT2. It functions as an intracellular negative feedback regulation of IFN signaling through ISGylation and as a multifunctional extracellular regulator of NK cell proliferation and IFN-γ stimulation, DC maturation and up-regulation of E-cadherin, CD15 and CD86 expression, T cell secretion of IFN-γ, and macrophage secretion of proinflammatory cytokines 146 and induction of anti-HIV activity (Fig. 4*H*) (48). We therefore profiled the expression of all potentially related molecules in the ISG15 pathway. Expression levels of IR9, STAT1, and STAT2, all transcription factors controlling ISG15 expression, were increased in $CD14^{high}$ monocytes, especially proinflammatory monocytes from active VKH patients (Fig. 4 *I* and *J*). Conversely, expression levels of these factors were reduced in $CD16^{high}$ monocytes during active disease (Fig. 4 *I* and *J*). We then explored the secretion of molecules by downstream cells. In VKH patients, IFN-γ expression was increased in NK and T cells, CD86 was elevated in $CD14^{high}$ monocytes, CD1C DCs, and megakaryocyte progenitors, and CD15 was slightly up-regulated in plasma cells and megakaryocyte progenitors while secretion level of IL-10 was undetectable in these cells (Fig. 4*K*). Collectively, these scRNA-seq results suggested that up-regulated ISG15 expression in proinflammatory monocytes via activation of IR9, STAT1, and STAT2 may drive multiple effector cells to secret proinflammatory factors, resulting in VKH disease. Further, relatively long-term corticosteroid treatment (3 mo) reduced ISG15 expression. Corticosteroids can inhibit the activation of proinflammatory cytokines such as IFN-γ and proinflammatory transcription factors including STAT family members (49). Therefore, these results suggested that corticosteroids may inhibit the activation of ISG15 in convalescent patients to suppress the production of IFN-γ and the ensuing activation of STAT1 and STAT2, thereby restraining disease activity.

Discussion

In the present study, we provide an insight into the human circulating monocytes of healthy individuals and autoimmune uveitis patients at single-cell resolution. Remarkably, we identified six subsets with unique gene expression patterns in healthy human blood monocytes and provide a further and more precise subdivision of existing monocyte categories. Moreover, our findings uncovered that the gene expression signatures, activation states, and up/down-stream pathways of referred monocyte subpopulations in VKH patients were significantly alternated when compared with healthy individuals. We also identified ISG15 as a disease-specific signature preferentially enriched in the proinflammatory subset from VKH patients.

Monocytes are a major component of human peripheral blood cells, with critical functions in antigen presentation, pathogen sensing, and phagocytosis (50), but functional heterogeneity among subsets is poorly understood. Herein, we utilized negative selection by microbeads to collect monocytes from human peripheral blood and defined phenotypes and putative functions by scRNA-seq and functional annotation. We identified 11 clusters in peripheral blood based on the expression of established cell lineage markers detected by scRNA-seq: $CD14^{high}$ monocytes, $CD16^{high}$ monocytes, T lymphocytes, B lymphocytes, plasma cells, NK cells, NKT cells, megakaryocyte progenitors, $CD1c^{+}$ DCs, pDCs, and a population of unknown identity. Further analysis of gene expression patterns revealed several markers for $CD14^{high}$ monocytes (*CSTA, MS4A6A, CXCL8, CTSS, LGALS1, LGALS2,* and *CST3*) and $CD16^{high}$ monocytes (*CDKN1C, HES4, SMIM25, MTSS1, BCL2A1,* and *RRAS*). This analysis also identified other cell types in human peripheral blood with marker expression profiles similar to monocytes. Like monocytes, DCs, B lymphocytes, and plasma cells expressed many of the same HLA class II genes, consistent with functions as antigen-presenting cells. Further, $CD16^{high}$ monocytes expressed many genes in common with other cell types, including *RHOC* expressed by $CD1c^{+}$ DCs, NK cells, and NKT cells, suggesting shared functions of these genes in actin dynamics, vesicular trafficking, gene transcription, cell cycle progression, and cell adhesion (51). The gene encoding *CD79B*, which served as the signal transducing subunit of the B cell receptor (52), was also expressed by $CD16^{high}$ monocytes, disputing the original idea that CD79B is only expressed on the surface of B lymphocytes. The shared expression of *FCGR3A*/CD16 by $CD16^{high}$ monocytes, NK cells, and NKT cells was consistent with previous findings that *FCGR3A* encoded a receptor important for antibody-dependent NK cell-mediated cytotoxicity (53).

Human blood monocytes are traditionally divided into three populations: classical monocytes ($CD14^{++}$ $CD16^{-}$), intermediate monocytes ($CD14^{++}$ $CD16^{+}$), and nonclassical monocytes ($CD14^{dim}$ $CD16^{++}$), according to morphology and molecular markers detected by flow cytometry (54). However, the precision of this classification is biased by the limited number of known cellular markers. Here, we present an approach to characterize human monocyte subsets in unprecedented detail by scRNA-seq of 11,259 circulating monocytes from three human healthy individuals. This analysis revealed six distinct monocyte populations, five $CD14^{high}$ subpopulations in addition to the $CD16^{high}$ population. Alternatively, intermediate monocytes did not form a distinct population but were mainly distributed at the junction between $CD14^{high}$ and $CD16^{high}$ monocytes, suggesting that such cells are in the transition state between classical and nonclassical (55). We herein present an alternative classification consisting of six human monocyte populations according to cellular marker expression profile and unique functional annotation: S100A12 monocytes, HLA monocytes, CD16 monocytes, proinflammatory monocytes, megakaryocyte-like monocytes, and NK-like monocytes. The S100A12 monocytes demonstrated an expression profile similar to all other $CD14^{high}$ monocyte subsets, including

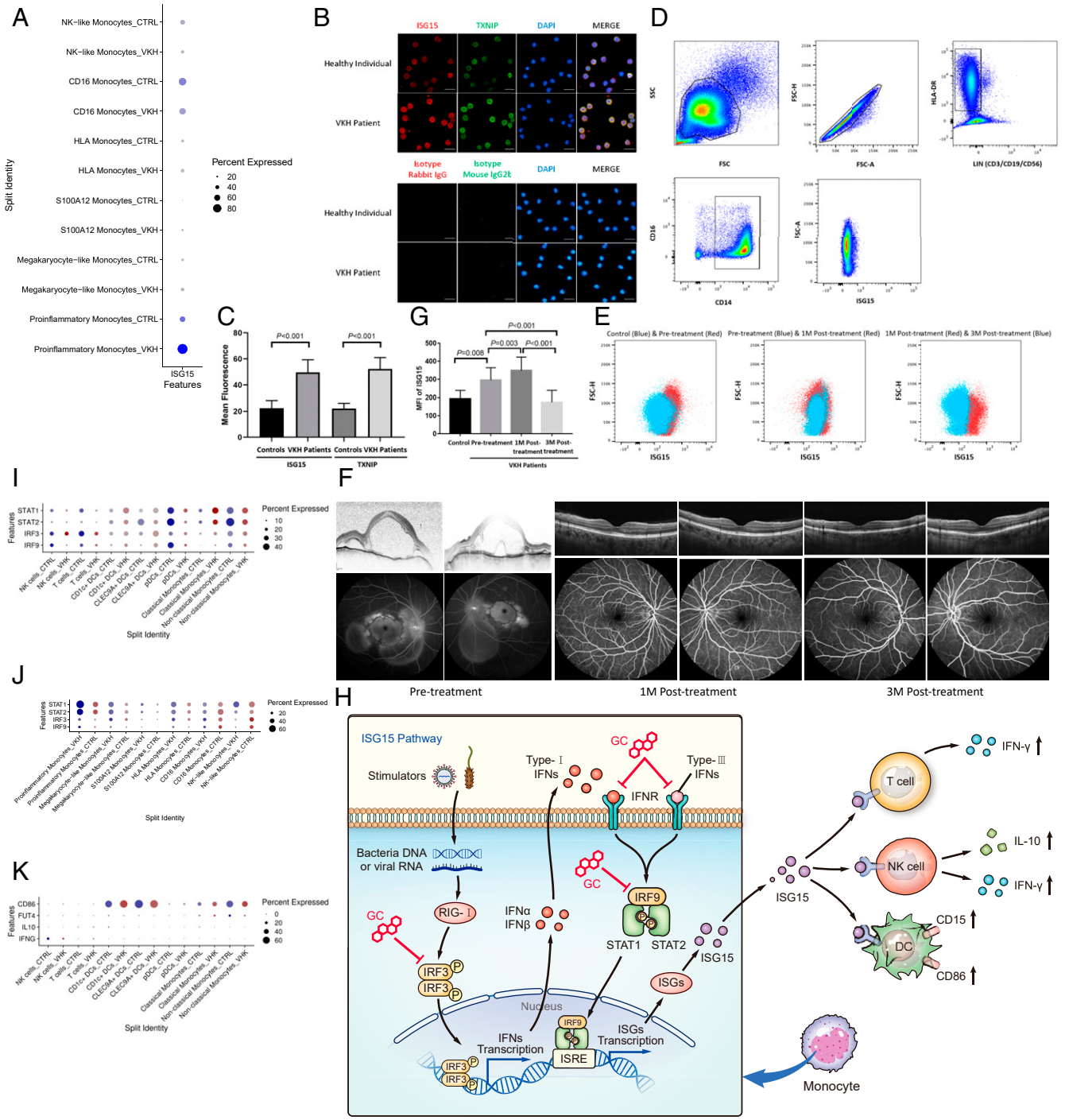

Fig. 4. The production of ISG15 in VKH patients was reduced after immunosuppressive therapy. (*A*) The dot plot shows the expression of ISG15 in monocyte subpopulations from VKH patients and healthy people. (*B*) Representative images of immunofluorescence staining targeting ISG15 (red) and TXNIP (green) in monocytes from active VKH patients ($n = 6$) and healthy controls ($n = 6$). (Scale bars: 20 μm.) (*C*) Quantification of ISG15 and TXNIP expression at the protein level. Each sample is quantified four images. (*D*) Gating strategy of $CD14^{high}$ monocytes $(LIN\_(CD3, CD19, CD56)^{-}\ HLA\text{-}DR^{+}\ CD14^{++})$. FSC, forward scattering; SSC, side scattering; A, area; H, height. (*E*) Flow cytometry shows the MFI of ISG15 of one healthy donor and one VKH patient in acute stage (*Left*), one VKH patient in acute and in convalescent stage after 1-mo corticosteroid treatment (*Middle*), and one VKH patient in acute and in convalescent stage after 3-mo corticosteroid treatment (*Right*). (*F*) Patient in acute stage before treatment: The OCT (*Top Left*, *Top Right*) and FFA (*Bottom Left*, *Bottom Right*) images show choroiditis, serous retinal detachment, disk edema, or exudative retinal detachment of both eyes in acute VKH patients. Patient in convalescent stage after 1-mo (1M) treatment: The OCT (*Top Left*, *Top Right*) and FFA (*Top Left*, *Top Right*) images of both eyes show no evidence of acute ocular inflammation, including choroiditis, serous retinal detachment, disk edema, or exudative retinal detachment in convalescent VKH patients after 1-mo corticosteroids treatment. Patient in convalescent stage after 3-mo (3M) treatment: The OCT (*Top Left*, *Top Right*) and FFA (*Bottom Left*, *Bottom Right*) images of both eyes in convalescent VKH patients after 3-mo corticosteroid treatment. (*G*) Bars show the MFI of ISG15 in healthy donors ($n = 6$), and acute VKH patients ($n = 8$) in acute and in convalescent stage after 1-mo and 3-mo corticosteroid treatment. (*H*) The ISG15 pathway and possible mechanisms by which glucocorticoids inhibit its production. The dot plot shows the expression of IRF3, IRF9, STAT1, and STAT2 in all cell clusters (*I*) and in monocyte subsets (*J*) from acute VKH patients and healthy controls. (*K*) The dot plot shows the expression of cytokines produced by downstream T cells (IFN-γ), NK cells (IFN-γ, IL-10), and DCs (CD15/FUT4, CD86) in all clusters from acute patients and healthy individuals. GC, glucocorticoid; IFNR, interferon receptors; ISRE, interferon-sensitive response element.

shared expression of *S100A12, S100A8,* and *S100A9*. The HLA monocytes exhibited the highest expression levels and the greatest number of different MHC class II molecules, implicating this subset in antigen presentation and downstream stimulation of $CD4^+$ T cells (56). More importantly, this subtype encompassed the intermediate monocytes with gene expression patterns indicative of a transition state from classical to nonclassical, thus providing a feasible strategy to study this transformation process. CD16 monocytes most closely resembled the well-defined nonclassical $CD16^{high}$ monocytes, including high expression of *FCGR3A*, but also expressed several population-specific (i.e., discriminative) genes, such as *CDKN1C, TCF7L2,* and *RHOC*. This expression profile suggested up-regulation of Notch and Wnt signaling pathways and negative regulation of cell proliferation. Proinflammatory monocytes also showed a unique gene expression signature, with high expression levels of *IL-1B, CCL3,* and *CCL4*, genes that orchestrate virus infection, inflammatory processes, and pyroptotic cell death. Megakaryocyte-like monocytes shared discriminative genes with megakaryocytes, such as *PPBP* and *PF4*, associated with platelet activation and inflammation. Finally, NK-like monocytes expressed the gene signature of NK cells (e.g., high expression levels of *NKG7, KLRB1, GNLY,* and *GZMA*) in addition to coexpressing a monocyte-typical gene set.

Human monocytes are critical innate immune cells that sense environmental changes, present antigens to downstream cells, and initiate immune responses in the pathology of a variety of autoimmune diseases, such as multiple sclerosis (MS) and inflammatory bowel disease (57, 58). VKH disease is a typical systemic autoimmune disease affecting both eyes that carries a high risk of blindness in the Asian population. Unlike many other autoimmune diseases, the inflamed intraocular tissue is difficult to obtain, limiting direct investigation of pathogenesis. Thus, our understanding of the immune processes in human uveitis has come mainly from studies on circulating immune cells. Although monocytes are essential initiators of autoimmunity in human uveitis, their exact functions, gene expression alterations, and activated states are still unclear. Firstly, our findings revealed a previously unexplored landscape of monocytes from human uveitis, VKH patients, compared with healthy individuals. Two subsets, CD16 and proinflammatory monocytes, evoked our attention for their distinguished changes of gene expression and the subpopulation signature in VKH disease. The marker gene of proinflammatory monocytes changed from *CCL4L2*-expressing in the normal state to *ISG15*-expressing in VKH disease patients, implying that this population had largely transitioned to the activated state. Furthermore, proinflammatory monocytes exhibited the largest number of differentially expressed genes (DEGs) among all subsets, with *RPS4Y1* and *TXNIP* showing the greatest up-regulation. Ribosomal protein S4, Y-linked 1 (RPS4Y1) initiated the activation of the Y chromosome, and its overexpression results in reduced trophoblast cell invasion and decreased STAT3 phosphorylation (40). STAT3 had potent antiinflammatory effects (59); thus the up-regulation of RPS4Y1 in proinflammatory monocytes may induce the inflammation in VKH patient through the suppression of STAT3. TXNIP mediated redox/glucose-induced stress and inflammation, and its up-regulation may suggest that this population was central to the promotion of inflammation in VKH disease patients. Proinflammatory monocytes also highly expressed *FOS, ISG15, LY6E,* and *MX1*, genes implicated in virus infection, type-I IFN signaling, and responses to IFN-gamma, providing the evidence to support the previous hypotheses that viral infection might provoke VKH disease through a mechanism of molecular mimicry. Therefore, our findings could indicate that viral infection irritated the proinflammatory monocytes acting as an initiator triggering the autoimmune response underlying VKH disease. Alternatively, the nonclassical-like CD16 monocytes highly expressed *RPS4Y1, S100A8,* and *S100A9*, which were considered critical alarmins that induce inflammation and promote the migration and chemotaxis of granulocytes and neutrophils (59), while these CD16 monocytes also showed markedly reduced expression levels of *CCL3, CCL4, TNF, IL1B,* and *NLRP3,* which regulated inflammatory responses and chemotaxis. Our comprehensive biological process analysis of CD16 monocytes showed that nonclassical subsets dually regulated the apoptotic signaling pathway, inflammatory response, and cell chemotaxis and migration in VKH disease, instead of simply promoting or inhibiting inflammation. Previous studies also reported that nonclassical monocytes had controversy toward the functions in different autoimmune diseases (60–63). Hence, these striking phenomena revealed that different subsets of monocytes contributed to distinctive functions during VKH disease, shedding high light onto the precise pathogenesis of autoimmune diseases.

Early and aggressive systemic corticosteroid administration is the mainstay treatment to reduce VKH disease activity and development (13). Therapeutic responses are monitored by clinical symptoms and ancillary tests, such as OCT (RTVue-100, Optovue Inc., Fremont, CA; Spectralis HRAOCT, Heidelberg Engineering, Heidelberg, Germany) or FFA (VISUCAM500, Carl Zeiss Meditec AG, Goeschwitzer, Germany) as there are no reliable disease-specific biomarkers to quantitatively evaluate the activity of human uveitis and treatment efficacy. In view of the pivotal roles of these defined proinflammatory monocytes, we screened for the potential biomarker and identified the top marker in this subset by analyzing scRNA-seq data, ISG15, an antiviral protein up-regulated after systemic IFN exposure, viral infection, and LPS treatment. Intracellular ISG15 can be induced by IFNs, and in turn prevent IFN-α/β overamplification and autoinflammation through ISGylation (48). ISG15 expression was significantly elevated in $CD14^{high}$ monocytes from acute VKH patients compared to healthy controls, verified by flow cytometry detection and immunofluorescent staining. After 3 mo of corticosteroid treatment, the level of ISG15 in VKH patients was normal, validating that ISG15 might reflect therapeutic effects. It was reported that IFNs induced ISG production, including ISG15, through STAT1/STAT2/IRF9 signaling. Furthermore, the corticosteroid was demonstrated to inhibit the expression of many proinflammatory cytokines, such as IFNs, and glucocorticoid receptors interfered with key proinflammatory transcription factors, such as the STAT family. Therefore, corticosteroid treatment down-regulated ISG15 production in monocytes from VKH patients possibly by suppressing its upstream initiators and transcription factors. Admittedly, our study has the limitation of a low sample capacity; we will expand the sample size in our further investigation.

In summary, based on an unbiased scRNA-seq approach, we built an atlas of human circulating monocytes with unprecedented resolution, discovered two monocyte subsets, and enabled a more complete understanding of monocytes in human peripheral blood. More strikingly, our study established the cell type-specific transcriptional programs of monocytes implicated in VKH patients and demonstrated the existence of previously unrecognized disease-associated proinflammatory monocytes, providing fundamental implications for the hypotheses of the pathogenesis of VKH disease. Furthermore, we identified that the disease-specific cell signature, ISG15, preferentially enriched in the proinflammatory monocyte subpopulation of VKH disease patients, might monitor disease activity and therapeutic response.

Materials and Methods

Subjects. Eleven patients with a diagnosis of initial acute bilateral VKH disease (five men and six women) and an average age of 44 y (43.50 ± 3.33) and six healthy individuals (three men and three women) with an average age of 32 y (32.17 ± 3.54) were included in this study. All study subjects were recruited in the Zhongshan Ophthalmic Centre from 3 October 2018 to 14 November 2019. Written informed consent was obtained from each patient or healthy individual for the genetic research studies and molecular testing. The diagnosis of VKH disease was based on the revised diagnostic criteria established by the First International Workshop on VKH Disease. These patients showed initial active uveitis without any treatment before blood drawing and were diagnosed based

on history, systemic examination, and ocular features on indirect ophthalmoscopy, OCT, and FFA. They received oral corticosteroid treatment with an initial dose of 80 to 100 mg/d and maintained for 2 wk. Then, oral corticosteroid treatment was tapered off gradually. After 1 mo of treatment with systemic corticosteroids, no evidence of acute ocular inflammation, including choroiditis, serous retinal detachment, disk edema, or exudative retinal detachment, was observed by clinical examination. Blood samples from VKH patients were obtained after 1-mo and 3-mo treatment, respectively. This study was performed in accordance with protocols formally reviewed and approved by the Ethics Committee of Zhongshan Ophthalmic Center (Guangzhou, China 2019KYPJ127).

Cell Isolation, Magnetic-Activated Cell Sorting, Flow Cytometry Staining, and Analysis. Fresh heparinized venous blood samples from healthy donors and VKH patients were processed within 2 h of collection. PBMCs were isolated from fresh blood using Ficoll density gradient centrifugation at 500 × *g* for 30 min at room temperature (25 °C). Single-cell suspensions were processed by a pan monocyte isolation kit according to the manufacturer's instructions (catalog no. 8804-6837-74; Thermo Fisher Scientific) in order to enrich monocytes as many as possible for scRNA-seq and flow cytometry. The purity of isolated monocytes detected by flow cytometry and scRNA-seq was 73.67% ± 3.16% and 72.15% ± 4.13%, respectively. The sorted cell suspensions were first stained per manufacturer recommendation with different panels of surface antibodies: CD3-FITC antibodies (catalog no. 561806; BD Biosciences), CD19-FITC antibodies (catalog no. 560994; BD Biosciences), CD56-FITC antibodies (catalog no. 562794; BD Biosciences), CD14-APC-H7 antibodies (catalog no. 560270; BD Biosciences), CD16-Alexa-Fluor647 antibodies (catalog no. 561724; BD Biosciences), and HLA-DR-BV421 antibodies (catalog no. 562805; BD Biosciences). After being incubated for 30 min and washed by phosphate-buffered saline (PBS) for two times, these surface-stained cells were proceeded by a BD Cytofix/Cytoperm Fixation/Permeabilization Solution Kit (catalog no. 554714; BD Biosciences) for staining intracellular ISG15. After a 30-min incubation and being washed by wash buffer for two times, cells were resuspended in 300 μL of PBS. Flow cytometry was performed on a BD Fortessa, and data were analyzed using FlowJo v10.1.

Monocyte Isolation and In Vitro Immunofluorescence. PBMCs were isolated from fresh heparinized venous blood from initial acute VKH patients without treatment and healthy individuals using Ficoll density gradient centrifugation. Single-cell suspensions were processed by a human $CD14^+$ positive selective kit according to the manufacturer's instructions (catalog no. 8802-6834-74; Thermo Fisher Scientific) to obtain monocytes of high purity. Sorted monocytes were resuspended in PBS and fixed with 4% paraformaldehyde in PBS for 20 min. The fixed cells were washed three times in PBS prior to being plated onto laminin-coated slides. Permeabilizations were carried out in 0.3% Triton X-100 for 10 min. After three washes with PBS, monocytes were blocked in a blocking buffer (5% normal goat serum) for 30 min at room temperature (24 °C). Primary antibodies of TXNIP (catalog no. ab232330; Abcam) and ISG15 (catalog no. ab227541; Abcam) and isotypes of mouse IgG2b and rabbit IgG (catalog no. ab221850 and catalog no. ab172730; Abcam,) for negative controls were diluted in buffer consisting of 5% bovine serum albumin (BSA) in PBS and incubated overnight at 4 °C. After three washes with PBST (1‰ TWEEN 20 in PBS), secondary antibodies of goat anti-rabbit IgG/Alexa Fluor 594 and Alexa Fluor 488 AffiniPure goat anti-mouse IgG (H+L) (catalog no. EM35143-01, EMAR; catalog no. bs-0295G-AF594; Bioss) were applied for 45 min at room temperature with treatment of light avoidance. To visualize the cell nuclei, the slips were incubated and mounted with DAPI Fluoromount-G Mounting Medium (catalog no. HNFD-02; HELIXGEN). Finally, cells were examined using an Olympus IX73 inverted microscope.

Statistics. Analysis of data of the MFI of ISG15 between healthy controls and acute VKH patients was compared using a *t* test (two-tailed). Analysis of data of the MFI of ISG15 among the group of acute VKH patients without treatment, 1-mo treatment group, and 3-mo treatment group was performed using one-way repeated measures ANOVA with Bonferroni adjustment. The data of mean fluorescence (MF) of ISG15 and TXNIP comparing active VKH patients with healthy donors were analyzed using one-way ANOVA. Statistical analysis was performed using IBM SPSS Statistics version 25, and bar plots were performed using Graphpad Prism 7.0 (GraphPad Software, Inc., La Jolla, CA).

scRNA-Seq. The single-cell populations with viability of more than 90% were loaded for scRNA-seq libraries preparation on the Chromium platform (10× Genomics, Pleasanton, CA) with single-cell gene expression 3′ V2 or 3′ V3 kits following the manufacturer's protocol. Briefly, single cells were partitioned by gel beads in EMulsion (GEMs) using the Chromium instrument, followed by cell lysis and barcoded reverse transcription of RNA, amplification, enzymatic fragmentation, 5′ adaptor attachment, and sample indexing. Libraries were sequenced on Illumina HiSeq 2500 platforms.

Computational Methods.

Alignment and quantification of the scRNA-seq data. Demultiplexing, alignment to the GRCh38 reference, and quantification of sequencing reads for each sample were performed using Cell Ranger (Version 3.0.2) with the default parameter. The filtered gene-barcode matrices for single cells were analyzed using Seurat (V3) following the tutorial at https://satijalab.org/seurat/v3.1/integration.html. Cells were filtered out with more than 15% of mitochondrial genes and fewer than 500 or greater than 10,000 detected genes.

Identifying major cell type in monocytes. Both normal and VKH datasets were from three biological replicates, and, depending on the enrichment method and individual differences, each sample contained different distributions of major cell types. To remove the batch effect, we integrated two datasets using canonical correlation analysis (CCA) of Seurat packages. After PCA to reduce dimensionality and build k-nearest neighbor graphs (k = 30) of the cells based on the Euclidean distance in the 46-dimensional PC space, the main cell cluster was identified using the Louvain–Jaccard graph-based method (with parameter set to "overcluster"). Next, we identified marker genes of each cluster and matched them with well-known PBMC classes, including monocytes, T cells, and B cells.

Defining a molecular atlas of human monocyte types. Following basic cell-type identification by scRNA-seq, we conducted further clustering analysis of $CD14^+$ and $CD16^+$ monocytes using the Seurat pipeline. In brief, the expression value of each gene was normalized using the LogNormalize method. The top 2,000 highest variability genes were selected by vst methods and used as input for PCA with reduced dimensionality. To partition the data into clusters of transcriptionally related cells, we used Louvain–Jaccard graphs based on the k-nearest neighbor method.

UMAP was used to reduce high-dimension into two-dimension (2D) for visualization.

Integrating normal and VKH scRNA-seq data. We extracted $CD14^+$ and $CD16^+$ monocyte clusters from scRNA-seq data of VKH patients and integrated these data with normal donor data using the Seurat label transfer pipeline.

Data Availability. The scRNA-seq data were deposited in the National Center for Biotechnology Information Gene Expression Omnibus (GEO) database (accession no. GSE148020) (64). All study data are included in the article, *SI Appendix*, and Datasets S1–S5.

ACKNOWLEDGMENTS. We thank Xiongze Zhang for his contribution to assist in some examinations of patients. This work was supported by grants from the Science and Technology Program of Guangzhou (201804010415) (to W.C.), the National Key R&D Program of China (2018YFA0108300 and 2017YFC1001300), and the National Natural Science Foundation of China (31700900) (to Youjin Hu). The funding organizations had no role in the design or conduct of this research.

1. S. Hou, N. Li, X. Liao, A. Kijlstra, P. Yang, Uveitis genetics. *Exp. Eye Res.* **190**, 107853 (2020).
2. G. A. D. O'Keefe, N. A. Rao, Vogt-Koyanagi-Harada disease. *Surv. Ophthalmol.* **62**, 1–25 (2017).
3. J. L. Davis *et al.*, HLA associations and ancestry in Vogt-Koyanagi-Harada disease and sympathetic ophthalmia. *Ophthalmology* **97**, 1137–1142 (1990).
4. S. Silpa-Archa, N. Silpa-Archa, J. M. Preble, C. S. Foster, Vogt-Koyanagi-Harada syndrome: Perspectives for immunogenetics, multimodal imaging, and therapeutic options. *Autoimmun. Rev.* **15**, 809–819 (2016).
5. P. Andersson *et al.*, Molecular mechanisms of IL-33-mediated stromal interactions in cancer metastasis. *JCI Insight* **3**, e122375 (2018).
6. Y. Yang *et al.*, The PDGF-BB-SOX7 axis-modulated IL-33 in pericytes and stromal cells promotes metastasis through tumour-associated macrophages. *Nat. Commun.* **7**, 11385 (2016).
7. H. Ji *et al.*, TNFR1 mediates TNF-α-induced tumour lymphangiogenesis and metastasis by modulating VEGF-C-VEGFR3 signalling. *Nat. Commun.* **5**, 4944 (2014).
8. A. K. Rana, Y. Li, Q. Dang, F. Yang, Monocytes in rheumatoid arthritis: Circulating precursors of macrophages and osteoclasts and, their heterogeneity and plasticity role in RA pathogenesis. *Int. Immunopharmacol.* **65**, 348–359 (2018).

9. M. C. Gjelstrup *et al*., Subsets of activated monocytes and markers of inflammation in incipient and progressed multiple sclerosis. *Immunol. Cell Biol.* **96**, 160–174 (2018).
10. J. H. Ko, H. J. Lee, H. J. Jeong, J. Y. Oh, Ly6C^{hi} monocytes are required for mesenchymal stem/stromal cell-induced immune tolerance in mice with experimental autoimmune uveitis. *Biochem. Biophys. Res. Commun.* **494**, 6–12 (2017).
11. P. Fang *et al*., Immune cell subset differentiation and tissue inflammation. *J. Hematol. Oncol.* **11**, 97 (2018).
12. L. Ziegler-Heitbrock, Blood monocytes and their subsets: Established features and open questions. *Front. Immunol.* **6**, 423 (2015).
13. C. Bonnet, J. B. Daudin, D. Monnet, A. Brézin, [Vogt-Koyanagi-Harada disease]. *J. Fr. Ophtalmol.* **40**, 512–519 (2017).
14. L. Heger *et al*., CLEC10A is a specific marker for human CD1c^{+} dendritic cells and enhances their toll-like receptor 7/8-induced cytokine secretion. *Front. Immunol.* **9**, 744 (2018).
15. M. A. Turman, T. Yabe, C. McSherry, F. H. Bach, J. P. Houchins, Characterization of a novel gene (NKG7) on human chromosome 19 that is expressed in natural killer cells and T cells. *Hum. Immunol.* **36**, 34–40 (1993).
16. J. Siewiera *et al*., Natural cytotoxicity receptor splice variants orchestrate the distinct functions of human natural killer cell subtypes. *Nat. Commun.* **6**, 10183 (2015).
17. E. Bongen, F. Vallania, P. J. Utz, P. Khatri, KLRD1-expressing natural killer cells predict influenza susceptibility. *Genome Med.* **10**, 45 (2018).
18. W. Holter, M. Schwarz, A. Cerwenka, W. Knapp, The role of CD2 as a regulator of human T-cell cytokine production. *Immunol. Rev.* **153**, 107–122 (1996).
19. D. Sinha, A. Kumar, H. Kumar, S. Bandyopadhyay, D. Sengupta, dropClust: efficient clustering of ultra-large scRNA-seq data. *Nucleic Acids Res.* **46**, e36 (2018).
20. A. Hajas *et al*., Derailed B cell homeostasis in patients with mixed connective tissue disease. *Hum. Immunol.* **74**, 833–841 (2013).
21. K. Pieper, B. Grimbacher, H. Eibel, B-cell biology and development. *J. Allergy Clin. Immunol.* **131**, 959–971 (2013).
22. A.-C. Villani *et al*., Single-cell RNA-seq reveals new types of human blood dendritic cells, monocytes, and progenitors. *Science* **356**, eaah4573 (2017).
23. S. Wang *et al*., S100A8/A9 in inflammation. *Front. Immunol.* **9**, 1298 (2018).
24. T.-L. Tang-Huau *et al*., Human in vivo-generated monocyte-derived dendritic cells and macrophages cross-present antigens through a vacuolar pathway. *Nat. Commun.* **9**, 2570 (2018).
25. M. Nishida, J. Saegusa, S. Tanaka, A. Morinobu, S100A12 facilitates osteoclast differentiation from human monocytes. *PLoS One* **13**, e0204140 (2018).
26. J. A. Briggs, G. R. Burrus, B. D. Stickney, R. C. Briggs, Cloning and expression of the human myeloid cell nuclear differentiation antigen: Regulation by interferon alpha. *J. Cell. Biochem.* **49**, 82–92 (1992).
27. S.-M. Ong *et al*., A novel, five-marker alternative to CD16-CD14 gating to identify the three human monocyte subsets. *Front. Immunol.* **10**, 1761 (2019).
28. P. Thomas, A. Pranatharthi, C. Ross, S. Srivastava, RhoC: A fascinating journey from a cytoskeletal organizer to a cancer stem cell therapeutic target. *J. Exp. Clin. Cancer Res.* **38**, 328 (2019).
29. I. C. Taylor *et al*., Disrupting NOTCH slows diffuse intrinsic pontine glioma growth, enhances radiation sensitivity, and shows combinatorial efficacy with bromodomain inhibition. *J. Neuropathol. Exp. Neurol.* **74**, 778–790 (2015).
30. S. K. Narayana *et al*., The interferon-induced transmembrane proteins, IFITM1, IFITM2, and IFITM3 inhibit hepatitis C virus entry. *J. Biol. Chem.* **290**, 25946–25959 (2015).
31. X. Chen *et al*., The diabetes gene and Wnt pathway effector TCF7L2 regulates adipocyte development and function. *Diabetes* **67**, 554–568 (2018).
32. A. S. Brown *et al*., MTSS1/Src family kinase dysregulation underlies multiple inherited ataxias. *Proc. Natl. Acad. Sci. U.S.A.* **115**, E12407–E12416 (2018).
33. K. S. Borges, V. A. Arboleda, E. Vilain, Mutations in the PCNA-binding site of CDKN1C inhibit cell proliferation by impairing the entry into S phase. *Cell Div.* **10**, 2 (2015).
34. J. P. Moore, P. J. Klasse, HIV-1 pathogenesis: The complexities of the CCR5-CCL3L1 complex. *Cell Host Microbe* **2**, 281–283 (2007).
35. M. S. J. Mangan *et al*., Targeting the NLRP3 inflammasome in inflammatory diseases. *Nat. Rev. Drug Discov.* **17**, 688 (2018).
36. R. Colobran, E. Pedrosa, L. Carretero-Iglesia, M. Juan, Copy number variation in chemokine superfamily: The complex scene of CCL3L-CCL4L genes in health and disease. *Clin. Exp. Immunol.* **162**, 41–52 (2010).
37. M. A. Kowalska, L. Rauova, M. Poncz, Role of the platelet chemokine platelet factor 4 (PF4) in hemostasis and thrombosis. *Thromb. Res.* **125**, 292–296 (2010).
38. H. Wang, D. Liu, H. Zhang, Investigation of the underlying genes and mechanism of macrophage-enriched ruptured atherosclerotic plaques using bioinformatics method. *J. Atheroscler. Thromb.* **26**, 636–658 (2019).
39. C.-H. Wu *et al*., Extracellular vesicles derived from natural killer cells use multiple cytotoxic proteins and killing mechanisms to target cancer cells. *J. Extracell. Vesicles* **8**, 1588538 (2019).
40. X. Chen *et al*., Dysregulated expression of RPS4Y1 (ribosomal protein S4, Y-linked 1) impairs STAT3 (signal transducer and activator of transcription 3) signaling to suppress trophoblast cell migration and invasion in preeclampsia. *Hypertension* **71**, 481–490 (2018).
41. S. Nasoohi, S. Ismael, T. Ishrat, Thioredoxin-interacting protein (TXNIP) in cerebrovascular and neurodegenerative diseases: Regulation and implication. *Mol. Neurobiol.* **55**, 7900–7920 (2018).
42. C.-Y. Wang *et al*., Dl-3-n-Butylphthalide inhibits NLRP3 inflammasome and mitigates alzheimer's-like pathology via Nrf2-TXNIP-TrX Axis. *Antioxid. Redox Signal.* **30**, 1411–1431 (2019).
43. A. Greco *et al*., Vogt-Koyanagi-Harada syndrome. *Autoimmun. Rev.* **12**, 1033–1038 (2013).
44. K. L. Wong *et al*., Gene expression profiling reveals the defining features of the classical, intermediate, and nonclassical human monocyte subsets. *Blood* **118**, e16–e31 (2011).
45. J. Cros *et al*., Human CD14dim monocytes patrol and sense nucleic acids and viruses via TLR7 and TLR8 receptors. *Immunity* **33**, 375–386 (2010).
46. J. V. Dzimianski, F. E. M. Scholte, É. Bergeron, S. D. Pegan, ISG15: It's complicated. *J. Mol. Biol.* **431**, 4203–4216 (2019).
47. P. He *et al*., Screening of gene signatures for rheumatoid arthritis and osteoarthritis based on bioinformatics analysis. *Mol. Med. Rep.* **14**, 1587–1593 (2016).
48. Y.-C. Perng, D. J. Lenschow, ISG15 in antiviral immunity and beyond. *Nat. Rev. Microbiol.* **16**, 423–439 (2018).
49. D. W. Cain, J. A. Cidlowski, Immune regulation by glucocorticoids. *Nat. Rev. Immunol.* **17**, 233–247 (2017).
50. C. V. Jakubzick, G. J. Randolph, P. M. Henson, Monocyte differentiation and antigen-presenting functions. *Nat. Rev. Immunol.* **17**, 349–362 (2017).
51. E. Nomikou, M. Livitsanou, C. Stournaras, D. Kardassis, Transcriptional and post-transcriptional regulation of the genes encoding the small GTPases RhoA, RhoB, and RhoC: Implications for the pathogenesis of human diseases. *Cell. Mol. Life Sci.* **75**, 2111–2124 (2018).
52. J. A. Ackermann *et al*., Syk tyrosine kinase is critical for B cell antibody responses and memory B cell survival. *J. Immunol.* **194**, 4650–4656 (2015).
53. K. A. Sablik, N. H. R. Litjens, M. Klepper, M. G. H. Betjes, Increased CD16 expression on NK cells is indicative of antibody-dependent cell-mediated cytotoxicity in chronic-active antibody-mediated rejection. *Transpl. Immunol.* **54**, 52–58 (2019).
54. L. Ziegler-Heitbrock *et al*., Nomenclature of monocytes and dendritic cells in blood. *Blood* **116**, e74–e80 (2010).
55. R. M. Kratofil, P. Kubes, J. F. Deniset, Monocyte conversion during inflammation and injury. *Arterioscler. Thromb. Vasc. Biol.* **37**, 35–42 (2017).
56. P. A. Roche, K. Furuta, The ins and outs of MHC class II-mediated antigen processing and presentation. *Nat. Rev. Immunol.* **15**, 203–216 (2015).
57. A. Fani Maleki, S. Rivest, Innate immune cells: Monocytes, monocyte-derived macrophages and microglia as therapeutic targets for alzheimer's disease and multiple sclerosis. *Front. Cell. Neurosci.* **13**, 355 (2019).
58. D. Lissner *et al*., Monocyte and M1 macrophage-induced barrier defect contributes to chronic intestinal inflammation in IBD. *Inflamm. Bowel Dis.* **21**, 1297–1305 (2015).
59. C. E. Egwuagu, STAT3 in CD4+ T helper cell differentiation and inflammatory diseases. *Cytokine* **47**, 149–156 (2009).
60. D. Chuluundorj, S. A. Harding, D. Abernethy, A. C. La Flamme, Expansion and preferential activation of the CD14(+)CD16(+) monocyte subset during multiple sclerosis. *Immunol. Cell Biol.* **92**, 509–517 (2014).
61. K. J. Woollard, F. Geissmann, Monocytes in atherosclerosis: Subsets and functions. *Nat. Rev. Cardiol.* **7**, 77–86 (2010).
62. K. Ley, Y. I. Miller, C. C. Hedrick, Monocyte and macrophage dynamics during atherogenesis. *Arterioscler. Thromb. Vasc. Biol.* **31**, 1506–1516 (2011).
63. G. Thomas, R. Tacke, C. C. Hedrick, R. N. Hanna, Nonclassical patrolling monocyte function in the vasculature. *Arterioscler. Thromb. Vasc. Biol.* **35**, 1306–1316 (2015).
64. Y. Hu, Y. Xiao, Genetic landscape and autoimmunity of monocytes in developing Vogt–Koyanagi–Harada disease. National Center for Biotechnology Information *Gene Expression Omnibus* (GEO) database. https://www.ncbi.nlm.nih.gov/geo/. Deposited 22 September 2020.